EPR Spectra of $[Cr(CO)_2L(\eta\text{-}C_6Me_6)]^+$ (L = PEt_3, PPh_3, $P(OEt)_3$, $P(OPh)_3$): Analysis of Line Widths and Determination of Ground State Configuration from Interpretation of ^{31}P Couplings

Michael P. Castellani,[†] Neil G. Connelly,[‡] Robert D. Pike,[§,||] Anne L. Rieger,[§] and Philip H. Rieger*[,§]

Department of Chemistry, Marshall University, Huntington, West Virginia 25755, School of Chemistry, University of Bristol, Bristol BS8 1TS, U.K., and Department of Chemistry, Brown University, Providence, Rhode Island 02912

Received March 24, 1997[⊗]

The preparation and characterization of $[Cr(CO)_2L(\eta\text{-}C_6Me_6)]$ (L = PEt_3, PPh_3, $P(OEt)_3$ and $P(OPh)_3$, are reported. One-electron oxidation affords unstable Cr(I) cations, $[Cr(CO)_2L(\eta\text{-}C_6Me_6)]^+$, EPR spectra of which are reported. Detailed analysis of the anisotropic ^{31}P hyperfine interaction indicates that, in frozen CH_2Cl_2/THF, the phosphine and phosphite complexes have $^2A'$ and $^2A''$ ground states, respectively. The hyperfine anisotropy can be accounted for by dipolar interaction of the ^{31}P nucleus with spin density on Cr and, in the case of the phosphite complexes, with ~0.01 P $3p_y$ spin density resulting from π-backbonding. Line width anomalies observed in EPR spectra of these and other Cr(I) and Mn(II) "piano stool" complexes can be understood in terms of molecular distortions resulting from solvation in frozen solutions.

Introduction

The ground state electronic configuration of Cr(I) "piano-stool" complexes such as $[Cr(CO)_2L(\eta\text{-}C_5R_5)]$, L = CO, phosphine, or phosphite, has been the subject of considerable experimental and theoretical interest. The parent tricarbonyl complexes are orbitally degenerate in idealized C_{3v} geometry and thus undergo a Jahn−Teller distortion to C_s symmetry and either a $^2A'$ or $^2A''$ ground state.[1] EPR spectroscopic studies of $[Cr(CO)_3(\eta\text{-}C_5H_5)]$[2] and $[Cr(CO)_3(\eta\text{-}C_5Me_5)]$,[1] doped into single crystals of the Mn(I) analogs, indicated $^2A'$ and $^2A''$ ground states, respectively. An LCAO-HFS-MO study[1] of $[Cr(CO)_3(\eta\text{-}C_5H_5)]$ showed that the two ground states differ primarily in the OC−Cr−CO bond angles: the optimum conformation for $^2A'$ has angles of 85, 100, and 100° whereas $^2A''$ has angles of 92, 84, and 84°. An EPR study of $[Cr(CO)_3(\eta\text{-}C_5Ph_5)]$ in frozen toluene suggested the possibility of two conformations in temperature-dependent equilibrium.[3] The single-crystal X-ray structure of this complex[3] showed two somewhat differently distorted molecules per unit cell; the OC−Cr−CO bond angles of the two molecules match approximately the predictions of Fortier et al.[1] for the ground state conformations corresponding to $^2A'$ and $^2A''$.[4] Thus, small environmental effects can lead to either ground state for the tricarbonyl complexes.

EPR studies of the phosphine-substituted complexes, $[Cr(CO)_2(PPh_3)(\eta\text{-}C_5H_5)]$[5] and $[Cr(CO)_2(PMe_3)(\eta\text{-}C_5Me_5)]$,[1] doped into single crystals of the Mn(I) analogs, indicated a $^2A''$ ground state for both complexes, but the LCAO-HFS-MO study of Fortier et al.[1] showed that the $^2A'$ state lies only 15 kJ mol^{-1} higher in energy, corresponding to opening of the OC−Cr−CO bond angle from 83 to 100°. Thus, environmental effects may well dictate the ground state of a phosphine- or phosphite-substituted complex. The reason for the bond angle dependence of ground state is easily understood: π-overlap of the metal d-orbitals with CO π-acceptor orbitals changes significantly with the OC−Cr−CO angle. The effect on the singly occupied MO (SOMO) and the two highest energy doubly occupied MOs, computed using extended Hückel MO theory,[6] is shown in Figure 1 for the optimized $^2A'$ and $^2A''$ structures of Fortier et al.[1] The interchange of the SOMO and HOMO is clearly a result of better π-overlap of the a″ MO and poorer overlap of the *a*′ MO with increasing bond angle.

The ^{31}P hyperfine couplings observed in EPR spectra of transition metal complexes with phosphorus ligands hold potentially important information relating to molecular and electronic structure. In a recent paper,[7] we were able to make some progress in the interpretation of the isotropic ^{31}P couplings observed in spectra of octahedral Cr(I) carbonylphosphine and -phosphonite complexes. Unfortunately, the spectra of these complexes were not sufficiently well resolved to enable the

[†] Marshall University.
[‡] University of Bristol.
[§] Brown University.
[||] Present address: Department of Chemistry, College of William and Mary, Williamsburg, VA 23185.
[⊗] Abstract published in *Advance ACS Abstracts,* September 15, 1997.

(1) Fortier, S.; Baird, M. C.; Preston, K. F.; Morton, J. R.; Ziegler, T.; Jaeger, T. J.; Watkins, W. C.; MacNeil, J. H.; Watton, K. A.; Hensel, K.; Le Page, Y.; Charland, J.-P.; Williams, A. J. *J. Am. Chem. Soc.* **1991**, *113*, 542.
(2) Krusic, P. J.; McLain, S. J.; Morton, J. R.; Preston, K. F.; Le Page, Y. *J. Magn. Reson.* **1987**, *74*, 72. Morton, J. R.; Preston, K. F. Cooley, N. A.; Baird, M. C.; Krusic, P. J.; McLain, S. J. *J. Chem. Soc., Faraday Trans. 1* **1987**, *83*, 3535.
(3) Hoobler, R. J.; Hutton, M. A.; Dillard, M. M.; Castellani, M. P.; Rheingold, A. L.; Rieger, A. L.; Rieger, P. H.; Richards, T. C.; Geiger, W. E. *Organometallics* **1993**, *12*, 116.
(4) Extended Hückel MO calculations based on the coordinates of the two structures confirm that one is $^2A'$ and the other $^2A''$.
(5) Cooley, N. A.; Baird, M. C.; Morton, J. R.; Preston, K. F.; Le Page, Y. *J. Magn. Reson.* **1988**, *76*, 325.
(6) EHMO calculations used the Alvarez collected parameters supplied with the CACHE software. CACHE Scientific, Beaverton, OR.
(7) Cummings, D. A.; McMaster, J.; Rieger, A. L.; Rieger, P. H. *Organometallics* **1997**, *16*, 4362.

S0276-7333(97)00251-3 CCC: $14.00

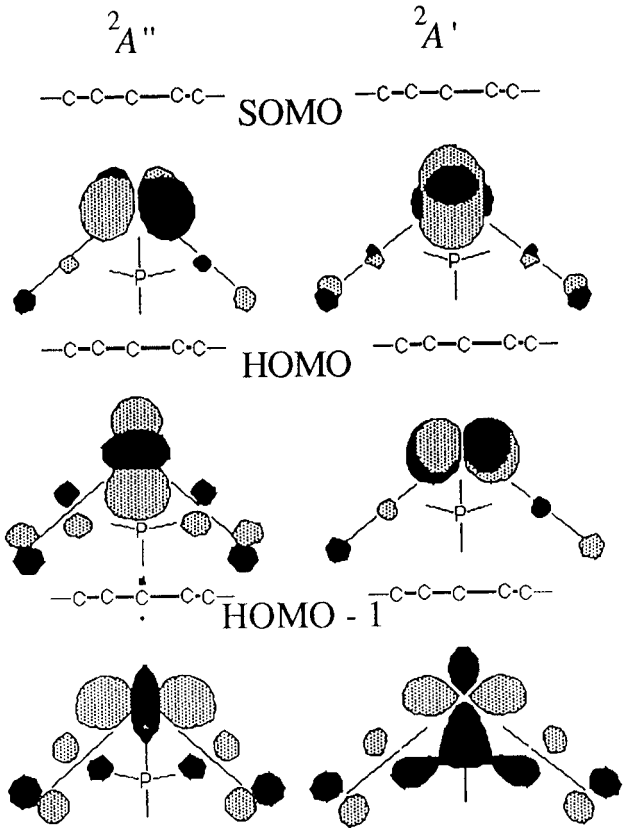

Figure 1. The three highest energy occupied MOs, computed using extended Hückel MO theory, for the conformations of $[Cr(CO)_2(PH_3)(\eta\text{-}C_5H_5)]$ found to give $^2A''$ and $^2A'$ ground states.

accurate measurement of the ^{31}P hyperfine anisotropies. Since each *g*-feature in spectra of $[Cr(CO)_2L(\eta\text{-}C_5R_5)]$ and $[Cr(CO)_2L(\eta\text{-}C_6R_6)]^+$ is a simple ^{31}P doublet, spectra of these complexes offer a better opportunity to obtain accurate measures of ^{31}P hyperfine anisotropies. Unfortunately, except for L = $PPhMe_2$, spectra of $[Cr(CO)_2L(\eta\text{-}C_5Ph_5)]$[8] are marred by anomalously broad low-field features which limited the accuracy of measurement of the ^{31}P splitting. The dilute single-crystal studies of $[Cr(CO)_2(PPh_3)(\eta\text{-}C_5H_5)]$[5] and $[Cr(CO)_2(PMe_3)(\eta\text{-}C_5Me_5)]$[1] did not employ enough orientations to determine accurately the ^{31}P hyperfine matrices. The cationic analogs reported here, $[Cr(CO)_2L(\eta\text{-}C_6Me_6)]^+$ (L = PEt_3, PPh_3, $P(OEt)_3$, and $P(OPh)_3$) proved to exhibit spectra with sufficiently sharp features that complete accurate measurement of the ^{31}P coupling matrices was possible. As we will show below, detailed interpretation remains nontrivial, largely because of the uncertainty in the orientation of the hyperfine matrix principal axes, but substantial progress is possible, both in understanding the origins of the ^{31}P hyperfine couplings and in assigning electronic ground states to the observed radical species.

The electronic structure insights discussed above lead to a semiquantitative understanding of the anomalous variation of component widths observed in frozen solution EPR spectra of $[Cr(CO)_2L(\eta\text{-}C_6Me_6]^+$ and other Cr(I)[8] and Mn(II)[9] piano stool complexes.

Table 1. Analytical, IR Spectroscopic, and Electrochemical Data for $[Cr(CO)_2L(\eta\text{-}C_6Me_6)]$

		analysis[a] (%)			
L	color	C	H	IR[b]/cm^{-1} ν(CO)	$E^{o\prime}$/V[c]
PEt_3	yellow	61.8 (61.9)	8.4 (8.5)	1849, 1788	−0.09
PPh_3	orange	*d*	*d*	1858, 1797	0.03
$P(OEt)_3$	yellow	55.1 (55.0)	7.8 (7.6)	1868, 1806	0.10
$P(OPh)_3$	yellow	66.2 (66.2)	5.7 (5.7)	1887, 1826	0.32

[a] Calculated values in parentheses. [b] In CH_2Cl_2. [c] In CH_2Cl_2 at a platinum disk electrode. Under the conditions used, the potential for the couple $[Fe(\eta\text{-}C_5H_5)_2]^+$−$[Fe(\eta\text{-}C_5H_5)_2]$ is 0.47 V. [d] Prepared as in ref 12.

Experimental Section

The preparation, purification, and reactions of the complexes described were carried out under an atmosphere of dry nitrogen or argon using dried, distilled, and deoxygenated solvents. The compounds $[Cr(CO)_2L(\eta\text{-}C_6Me_6)]$ were prepared by the UV photolysis of $[Cr(CO)_3(\eta\text{-}C_6Me_6)]$ in the presence of L (L = PPh_3,[10] PhC≡CPh[11]) or by the thermal displacement of PhC≡CPh from $[Cr(CO)_2(PhC{\equiv}CPh)(\eta\text{-}C_6Me_6)]$ by L.[12] IR spectra were recorded on a Nicolet 5ZDX FT spectrometer. Electrochemical studies were carried out in CH_2Cl_2 using an EG&G Model 273 potentiostat in conjunction with a three-electrode cell. For cyclic voltammetry, the auxiliary electrode was a platinum wire and the working electrode a platinum disk. The reference was an aqueous saturated calomel electrode (SCE) separated from the test solution by a fine-porosity frit and an agar bridge saturated with KCl. Solutions were 0.1×10^{-3} mol dm^{-3} in the test compound and 0.1 mol dm^{-3} in $[NBu_4][PF_6]$ as the supporting electrolyte. Under these conditions, $E^{o\prime}$ for the one-electron oxidation of $[Fe(\eta\text{-}C_5H_5)_2]$, added to the test solutions as an internal calibrant, is 0.47 V. Microanalyses were carried out by the staff of the Microanalytical Service of the School of Chemistry, University of Bristol.

Synthesis of $[Cr(CO)_2\{P(OPh)_3\}(\eta\text{-}C_6Me_6)]$. A mixture of $[Cr(CO)_2(PhC{\equiv}CPh)(\eta\text{-}C_6Me_6)]$ (134 mg, 0.30 mmol) and $P(OPh)_3$ (93 mg, 0.30 mmol) in *n*-hexane (50 cm^3) was heated under reflux for 3 h. The resulting yellow solution was filtered hot and then allowed to cool to 0 °C. The yellow precipitate was separated from the mother liquors and then dried *in vacuo* to give $[Cr(CO)_2\{P(OPh)_3\}(\eta\text{-}C_6Me_6)]$, yield 102 mg (59%). The compound is air-stable in the solid state and dissolves in solvents such as CH_2Cl_2, thf, and toluene to give moderately air-sensitive solutions.

The complexes $[Cr(CO)_2L(\eta\text{-}C_6Me_6)]$ (L = $P(OEt)_3$, PEt_3) were prepared similarly in 30−50% yields after a reaction time of 24 h and partial removal of solvent from the filtered reaction mixture before cooling to 0 °C. They may be further purified, if necessary, by recrystallization from *n*-hexane. Analytical, IR spectroscopic, and electrochemical data for the three new compounds, as well as $[Cr(CO)_2(PPh_3)(\eta\text{-}C_6Me_6)]$, are given in Table 1.

The cations $[Cr(CO)_2L(\eta\text{-}C_6Me_6)]^+$ (L = PEt_3, PPh_3, $P(OEt)_3$, $P(OPh)_3$) were prepared by addition of solid $[Fe(\eta\text{-}C_5H_5)_2][BF_4]$ to a solution of the neutral complex in 1:2 CH_2Cl_2/THF under nitrogen; the solution was then transferred by syringe to a nitrogen-filled EPR tube and frozen. The formation of the cation was confirmed by IR spectroscopy on a separate aliquot. X-Band EPR spectra of CH_2Cl_2/THF glasses were recorded at 90 K using a Bruker ESP-300E spectrometer equipped with a Bruker variable-temperature accessory and a Hewlett Packard 5350B microwave frequency counter. The field calibration was checked by measuring the resonance of the diphenylpicrylhydrazyl (dpph) radical before each series of spectra. Occasion-

(8) Hammack, D. J.; Dillard, M. M.; Castellani, M. P.; Rheingold, A. L.; Rieger, A. L.; Rieger, P. H. *Organometallics* **1996**, *15*, 4791.
(9) Pike, R. D.; Rieger, A. L.; Rieger, P. H. *J. Chem. Soc., Faraday Trans. 1* **1989**, *85*, 3913.
(10) Strohmeier, W.; Hellmann, H. *Chem. Ber.* **1964**, *97*, 1877.
(11) Strohmeier, W.; Hellmann, H. *Chem. Ber.* **1965**, *98*, 1598.
(12) Connelly, N. G.; Demidowicz, Z.; Kelly, R. L. *J. Chem. Soc., Dalton Trans.* **1975**, 2335.

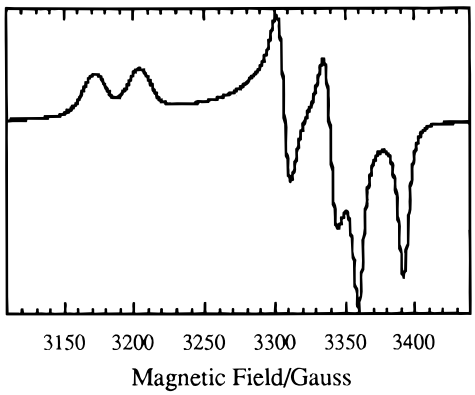

Figure 2. X-Band EPR spectrum of $[Cr(CO)_2(PEt_3)(\eta\text{-}C_6Me_6)]^+$ in CH_2Cl_2/THF (1:2) at 90 K.

ally spectra contained extra features attributed to radical decomposition products; in general, when the oxidation step was performed quickly and the solution immediately frozen, clean spectra free of extra features were obtained.

Results

EPR spectra of $[Cr(CO)_2L(\eta\text{-}C_6Me_6)]^+$ (L = PEt_3, PPh_3, $P(OEt)_3$, $P(OPh)_3$) at 90 K in frozen CH_2Cl_2/THF show three well-separated features corresponding to the three components of the **g**-matrix. Each feature is split into a doublet by hyperfine coupling to the ^{31}P nucleus. The spectrum of the PEt_3 derivative is shown in Figure 2, and EPR parameters are given in Table 2. The low-field features broadened somewhat as the temperature was increased, but the increase was less dramatic than in the case of $[Cr(CO)_2L(\eta\text{-}C_5Ph_5)]$.[8] Unlike the C_5Ph_5 complexes, which exhibited axial powder spectra at temperatures just above the melting point of the solvent, the spectra of $[Cr(CO)_2L(\eta\text{-}C_6Me_6)]^+$ collapsed into single broad lines when the solutions were melted. Room-temperature spectra of the L = PPh_3 and PEt_3 derivatives showed a variety of resonances, none of which could be associated with the frozen solution spectrum and thus apparently correspond to decomposition products. No attempt was made to record isotropic spectra of the L = $P(OEt)_3$ or $P(OPh)_3$ derivatives.

Discussion

g-Matrices. The **g**-matrices for $[Cr(CO)_2L(\eta\text{-}C_6Me_6)]^+$ are very similar to those of $[Cr(CO)_2L(\eta\text{-}C_5R_5)]$[1,5,8] and $[Mn(CO)_2(PPh_3)(\eta\text{-}C_5H_5)]^+$[9] with one component much larger than the free-electron value, a second component slightly larger than g_e, and a third component slightly smaller than g_e.

The frontier orbitals in d^5 piano stool complexes are essentially the octahedral t_{2g} set, two of a′ symmetry, eq 1a, and one of a″ symmetry, eq 1b. For a SOMO of

$$|k,a'\rangle = c_{k,x^2-y^2}|x^2-y^2\rangle + c_{k,z^2}|z^2\rangle + c_{k,xz}|xz\rangle + \ldots \quad (1a)$$

$$|k,a''\rangle = c_{k,yz}|yz\rangle + c_{k,xy}|xy\rangle \ldots \quad (1b)$$

a′ symmetry, g_{xx} and g_{zz} differ from g_e through spin−orbit coupling of the SOMO with the nearby a″ MO. Similarly g_{yy} is expected to be somewhat larger than g_e through coupling to the nearby a′ MO. The off-diagonal component, g_{xz}, also involves a′/a″ coupling. The resulting expressions are given by eqs 2. Since each sum

$$g_{xx} = g_e + \sum_{k\neq 0}\frac{\zeta}{\Delta E_{0k}} \times (c_{0,x^2-y^2}c_{k,yz} + \sqrt{3}c_{0,z^2}c_{k,yz} + c_{0,xz}c_{k,xy})^2 \quad (2a)$$

$$g_{yy} = g_e + \sum_{k\neq 0}\frac{\zeta}{\Delta E_{0k}}(c_{0,x^2-y^2}c_{k,xz} - \sqrt{3}c_{0,z^2}c_{k,xz} - c_{0,xz}c_{k,x^2-y^2} + \sqrt{3}c_{0,xz}c_{k,z^2})^2 \quad (2b)$$

$$g_{zz} = g_e + \sum_{k\neq 0}\frac{\zeta}{\Delta E_{0k}}(2c_{0,x^2-y^2}c_{k,xy} + c_{0,xz}c_{k,yz})^2 \quad (2c)$$

$$g_{xz} = \sum_{k\neq 0}\frac{\zeta}{\Delta E_{0k}}(c_{0,x^2-y^2}c_{k,yz} + \sqrt{3}c_{0,z^2}c_{k,yz} + c_{0,xz}c_{k,xy}) \times (2c_{0,x^2-y^2}c_{k,xy} + c_{0,xz}c_{k,yz}) \quad (2d)$$

contains only one important term, the off-diagonal term is approximately related to g_{xx} and g_{zz}, $g_{xz} \approx ((g_{xx} - g_e)(g_{zz} - g_e))^{1/2}$, so that the principal values are $g_X \approx g_e$, $g_Z \approx g_{zz} + g_{xx} - g_e$, consistent with the observed *g*-matrices with $g_X < g_Y < g_Z$.

On the other hand, for a SOMO of a″ symmetry, eqs 3 for g_{xx}, g_{zz}, and g_{xz} each have two major terms and

$$g_{xx} = g_e + \sum_{k\neq 0}\frac{\zeta}{\Delta E_{0k}} \times (c_{0,yz}c_{k,x^2-y^2} + \sqrt{3}c_{0,yz}c_{k,z^2} + c_{0,xy}c_{k,xz})^2 \quad (3a)$$

$$g_{yy} = g_e + \sum_{k\neq 0}\frac{\zeta}{\Delta E_{0k}}(c_{0,xy}c_{k,yz} - c_{0,yz}c_{k,xy})^2 \quad (3b)$$

$$g_{zz} = g_e + \sum_{k\neq 0}\frac{\zeta}{\Delta E_{0k}}(2c_{0,xy}c_{k,x^2-y^2} + c_{0,yz}c_{k,xz})^2 \quad (3c)$$

$$g_{xz} = \sum_{k\neq 0}\frac{\zeta}{\Delta E_{0k}}(2c_{0,xy}c_{k,x^2-y^2} + c_{0,yz}c_{k,xz}) \times (c_{0,xy}c_{k,xz} + \sqrt{3}c_{0,yz}c_{k,z^2} + c_{0,yz}c_{k,x^2-y^2}) \quad (3d)$$

that for g_{yy}, which involves coupling to more distant MOs of a″ symmetry, has no major terms. Thus g_{yy} should be close to g_e and may be slightly smaller than g_e as a result of coupling to distant empty MO's. In general, $g_{xz} < ((g_{xx} - g_c)(g_{zz} - g_e))^{1/2}$, so that $g_X > g_e$ but g_Z will still be large. Again, the predicted *g*-matrix is consistent with those observed.

In either case, the *X* and *Z* principal axes of the **g**-matrix are displaced from the molecular axes by the angle β_g, given by eq 4.

$$\tan 2\beta_g = \frac{2g_{xz}}{g_{zz} - g_{xx}} \quad (4)$$

The smallest **g**-component was found to correspond to the molecular *y*-axis (normal to the plane of symmetry) in dilute single-crystal spectra of $[Cr(CO)_2(PPh_3)(\eta\text{-}C_5H_5)]$[5] and $[Cr(CO)_2(PMe_3)(\eta\text{-}C_5Me_5)]$,[1] so that these complexes almost certainly have an $^2A''$ ground state. However, because the relative energies of the highest occupied MO's of a′ and a″ symmetry depend strongly

Table 2. EPR Parameters[a]

(a) Cr(I) Complexes

complex	g_1	g_2	g_3	A_1^P	A_2^P	A_3^P
$[Cr(CO)_2(PEt_3)(\eta\text{-}C_6Me_6)]^+$	1.993	2.025	2.110	30.4	32.1	31.1
$[Cr(CO)_2(PPh_3)(\eta\text{-}C_6Me_6)]^+$	1.993	2.026	2.102	29.6	31.5	30.7
$[Cr(CO)_2\{P(OEt)_3\}(\eta\text{-}C_6Me_6)]^+$	1.994	2.025	2.109	39.7	42.4	43.8
$[Cr(CO)_2\{P(OPh)_3\}(\eta\text{-}C_6Me_6)]^+$	1.993	2.024	2.112	40.0	42.4	43.1
$[Cr(CO)_2(PPhMe_2)(\eta\text{-}C_5Ph_5)]$[b]	1.994	2.013	2.106	32.6	34.8	34.2

(b) Mn(II) Complexes[c]

complex	g_1	g_2	g_3	A_1	A_2	A_3	β
$[Mn(CO)(dmpe)(\eta\text{-}C_5H_5)]^+$	2.000	2.021	2.187	35.6	≈0	115.3	45.5°
$[Mn(CO)_2(PBu_3)(\eta_5\text{-}6\text{-}exo\text{-}PhC_6H_6)^+$	2.009	2.014	2.090	12.1	≈0	105.1	13.5°

[a] Estimated accuracy: *g*-matrix components, ±0.001; *A*-matrix components, $\pm 0.2 \times 10^{-4}$ cm^{-1}. [b] Data from ref 8. [c] Data from ref 9.

on the OC−Cr−CO bond angle, we cannot assume a $^2A''$ ground state for similar complexes in different environments.

In our earlier work on $[Cr(CO)_2L(\eta\text{-}C_5Ph_5)]$,[8] we found axial powderlike spectra from low-temperature liquid solutions as a result of averaging of the molecular *x* and *y* axes through rotation of the "piano stool legs" with the very bulky C_5Ph_5 "seat" essentially stationary. From the shift of the g_Z features, we determined that the g_Z principal axis is displaced from the molecular *z* axis (normal to the C_5 ring) by $\beta_g \approx 15°$, but it was not possible to determine the direction of tilt, i.e., toward the phosphorus ligand or away from it. The C_6Me_6 ligand is not sufficiently bulky to give axial spectra in low-temperature liquid solutions, but a similar axis displacement is expected for $[Cr(CO)_2L(\eta\text{-}C_6Me_6)]^+$.

^{31}P Hyperfine Couplings. Examples of ^{31}P hyperfine coupling for phosphine or phosphite complexes can be divided into two classes: (i) Isotropic couplings on the order of $(20-40) \times 10^{-4}$ cm^{-1} and small anisotropies are observed in cases where the P atom lies on or near a SOMO nodal plane, e.g., in the octahedral V(0)[13] and Cr(I)[7] carbonyl phosphine complexes, analogous Mn(II) complexes,[14] and the species described in this paper; the coupling is probably negative and arises primarily from spin polarization of P 3s and inner-shell s-orbitals by spin density in a metal 3d orbital. (ii) Much larger isotropic couplings and relatively large anisotropies are often observed when the P atom is located on the *z*-axis and the SOMO is primarily a metal d_{z^2} orbital, e.g., $[Co(tpp)(PMe_3)]$, $\langle A^P\rangle = 222 \times 10^{-4}$ cm^{-1},[15] $[Rh_2(O_2CEt)_4(PPh_3)_2]^+$, $\langle A^P\rangle = 165 \times 10^{-4}$ cm^{-1},[16] and $[Co(C_2Ph_2)(CO)\{P(OEt)_3\}_2]$, $\langle A^P\rangle = 168 \times 10^{-4}$ cm^{-1};[17] in these cases, the isotropic and anisotropic couplings arise primarily from P 3s and $3p_z$ character, respectively. There are, however, several exceptions to these generalizations: thus $[W(CO)_4\{P(OMe)_3\}]^-$ exhibits a small isotropic coupling and relatively large anisotropy,[18] and some complexes with a phosphine on or near the *z* axis and metal d_{z^2} character show much smaller couplings, e.g., $[Mn(PMe_3)(\eta\text{-}C_4H_6)_2]$, $\langle A^P\rangle = 25 \times 10^{-4}$ cm^{-1} [19] and $[Rh_2(CO)_2(PPh_3)_2\{\mu\text{-}PhNC(Me)NPh\}_2]^+$, where no ^{31}P coupling is detectable.[20] Preston and co-workers[18] have attempted to rationalize some of these effects, but many of the details are not understood.

Here we focus our attention on the ^{31}P hyperfine anisotropy in spectra of $[Cr(CO)_2L(\eta\text{-}C_6Me_6)]^+$ as well as $[Cr(CO)_2(PPhMe_2)(\eta\text{-}C_5Ph_5)]$.[8] There are two potential sources of hyperfine anisotropy: (1) dipolar coupling of the ^{31}P nucleus with spin density on Cr (major axis *Z′* along the Cr−P bond); (2) dipolar coupling with spin density in a P 3p orbital. We assume that the P atom lies on the plane of symmetry (*xz*). If the SOMO has a″ symmetry, P $3p_y$ character is possible and may be significant for the phosphite ligands (major axis *Y′* normal to symmetry plane). Assuming that both anisotropic contributions are axial (i.e., that spin−orbit coupling corrections are negligible), the ^{31}P hyperfine components are given by eqs 5 where *a* and *b* are given

$$A_{X'} = \langle A\rangle - a - b \tag{5a}$$

$$A_{Y'} = \langle A\rangle - a + 2b \tag{5b}$$

$$A_{Z'} = \langle A\rangle + 2a - b \tag{5c}$$

by eqs 6 and 7. The point dipole approximation gives

$$a = \frac{P_{Cr}}{r^3}\rho_{3d}{}^{Cr} \tag{6}$$

$$b = \frac{2}{5}P_P\rho_{3p}{}^{P} \tag{7}$$

$P_{Cr} = 10.7 \times 10^{-4}$ cm^{-1}Å^3, and, according to Morton and Preston,[21] $P_P = 306 \times 10^{-4}$ cm^{-1}. For unit spin density on Cr and a Cr−P distance of 2.38 Å, we expect $a = 0.8 \times 10^{-4}$ cm^{-1}.

Since the **g**-matrix anisotropy is much greater than that of the hyperfine matrix, the observed features correspond to orientations along the **g**-matrix principal axes. In order to relate the ^{31}P hyperfine components of eqs 5 to the experimental results, we need the orientation of the hyperfine matrix principal axes relative to those of the **g**-matrix. We assume that the **g**-matrix *Y*-axis and hyperfine matrix *Y′* axis are normal

(13) McCall, J. M.; Morton, J. R.; Preston, K. F. *Organometallics* **1985**, *4*, 1272.
(14) Carriedo, G. A.; Connelly, N. G.; Perez-Carreno, E.; Orpen, A. G.; Rieger, A. L.; Rieger, P. H.; Riera, V.; Rosair, G. M. *J. Chem. Soc., Dalton Trans.* **1993**, 3103.
(15) Wayland, B. B.; Abd-Elmageed, M. E. *J. Am. Chem. Soc.* **1974**, *96*, 4809.
(16) Kawamura, T.; Fukamachi, K.; Hayashida, S. *J. Chem. Soc., Chem. Commun.* **1979**, 945.
(17) DeGray, J. A.; Meng, Qingjin; Rieger, P. H. *J. Chem. Soc., Faraday Trans. 1* **1987**, *83*, 3565.
(18) Hynes, R. C.; Preston, K. F.; Springs, J. J.; Williams, A. J. *J. Chem. Soc., Dalton Trans.* **1990**, 3655.
(19) McCall, J. M.; Morton, J. R.; Preston, K. F. *Organometallics* **1985**, *4*, 1272.
(20) Boyd, D. C.; Connelly, N. G.; Herbosa, G. G.; Hill, M. G.; Mann, K. R.; Mealli, C.; Orpen, A. G.; Richardson, K. E.; Rieger, P. H. *Inorg. Chem.*, **1994**, *33*, 960.

Table 3. Fitted Values of the ^{31}P Hyperfine Matrices[a]

(a) $g_{min} = g_Y$

complex	a	b	β_A	$A_{X'}$	$A_{Y'}$	$A_{Z'}$
$[Cr(CO)_2(PEt_3)(\eta\text{-}C_6Me_6)]^+$	0.8	0.8	33	−32.8	−30.4	−30.7
$[Cr(CO)_2(PPh_3)(\eta\text{-}C_6Me_6)]^+$	0.8	0.9	35	−32.3	−29.6	−29.9
$[Cr(CO)_2\{P(OEt)_3\}(\eta\text{-}C_6Me_6)]^+$	0.8	1.5	63	−44.3	−39.7	−41.9
$[Cr(CO)_2\{P(OPh)_3\}(\eta\text{-}C_6Me_6)]^+$	0.8	1.3	53	−44.0	−40.0	−41.3
$[Cr(CO)_2(PPhMe_2)(\eta\text{-}C_5Ph_5)]$	0.8	1.0	38	−35.7	−32.6	−33.3

(b) $g_{min} = g_X$

complex	a	β_A	$A_{X'}$	$A_{Y'}$	$A_{Z'}$
$[Cr(CO)_2(PEt_3)(\eta\text{-}C_6Me_6)]^+$	0.9	52	−32.1	−32.1	−29.4
$[Cr(CO)_2(PPh_3)(\eta\text{-}C_6Me_6)]^+$	0.9	57	−31.5	−31.5	−28.8
$[Cr(CO)_2\{P(OEt)_3\}(\eta\text{-}C_6Me_6)]^+$	0.4		−43.0	−42.4	−40.6
$[Cr(CO)_2\{P(OPh)_3\}(\eta\text{-}C_6Me_6)]^+$	0.6		−42.7	−42.4	−40.3
$[Cr(CO)_2(PPhMe_2)(\eta\text{-}C_5Ph_5)]$	0.9	63	−34.7	−34.8	−32.0

[a] Hyperfine couplings in units of 10^{-4} cm^{-1}.

to the reflection plane and thus collinear. The Cr−P bond axis (the hyperfine Z' axis) is oriented 134° from the Cr−C_5 axis in $[Cr(CO)_2(PMe_3)(\eta\text{-}C_5Ph_5)]$, and the g-matrix Z axis is displaced $\beta_g = \pm 15°$ from this axis.[8] Assuming similar angles for $[Cr(CO)_2L(\eta\text{-}C_6Me_6)]^+$, the hyperfine Z' axis is displaced from the **g**-matrix Z-axis by $\beta_A \approx 46 \pm 15°$. The observed splittings, A_X and A_Z, then are related to the principal values, $A_{X'}$ and $A_{Z'}$ by eqs 8.

$$A_X = \sqrt{A_{X'}^2 \cos^2 \beta_A + A_{Z'}^2 \sin^2 \beta_A} \qquad (8a)$$

$$A_Z = \sqrt{A_{X'}^2 \sin^2 \beta_A + A_{Z'}^2 \cos^2 \beta_A} \qquad (8b)$$

If we assume an a″ SOMO, so that $g_{min} = g_Y$, and $a \approx 0.8 \times 10^{-4}$ cm^{-1}, eqs 5 give the values of b, $A_{X'}$, and $A_{Z'}$ listed in Table 3a; the values of β_A were obtained from $A_{X'}$ and $A_{Z'}$ using eqs 8. The parameter b suggests P $3p_y$ spin densities on the order of 0.011 for the phosphites and 0.007 for the phosphines. Extended Hückel MO calculations[6] on the model compounds $[Cr(CO)_2(PH_3)(\eta\text{-}C_6H_6)]^+$, $[Cr(CO)_2\{P(OH)_3\}(\eta\text{-}C_6H_6)]^+$, and $[Cr(CO)_2(PH_3)(\eta\text{-}C_5H_5)]$ suggest a $3p_y$ spin density of ∼0.005 for $P(OH)_3$ but essentially no P $3p_y$ character for PH_3. Thus, a spin density of 0.011 for the phosphites is plausible, but 0.007 for the phosphines is much larger than anticipated. The values of the noncoincidence angle β_A are in good agreement with those expected, i.e., either ∼31 or ∼61°, but it is puzzling to find one angle for the phosphines and the other for the phosphites. Such a result would suggest different signs for g_{xz} for the phosphine and phosphite complexes, a conclusion difficult to rationalize in terms of a MO description of these complexes.

Alternatively, if we assume that the SOMO has a' symmetry so that $g_{min} = g_X$ and $b = 0$ (P $3p_y$ character is forbidden for an a' SOMO), the phosphite data cannot be fitted to eqs 8; however, the phosphine data give an entirely sensible fit with $a = 0.9 \times 10^{-4}$ cm^{-1} and $\beta_A \approx 60°$ (Table 3b).

Considering the parameters a, b, and β, the most satisfactory results are obtained by assuming $g_{min} = g_Y$ for the phosphites and $g_{min} = g_X$ for the phosphines. As we have seen, this implies a $^2A''$ ground state for the phosphites but $^2A'$ for the phosphines. A difference in ground state symmetry is surprising given the very similar **g**-matrices for the five complexes, but as we have pointed out above, very similar **g**-matrices are expected for $^2A'$ and $^2A''$.

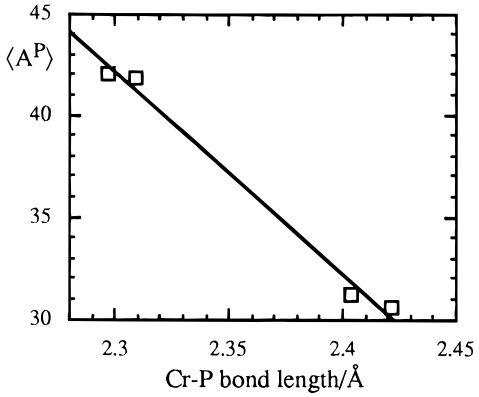

Figure 3. Average ^{31}P coupling for $[Cr(CO)_2L(\eta\text{-}C_6Me_6)]^+$, L = $P(OEt)_3$, $P(OPh)_3$, PEt_3, and PPh_3, as a function of Cr−P bond length in $[Cr(CO)_5L]$.

In our earlier paper,[7] we rationalized the isotropic ^{31}P couplings in octahedral Cr(I) carbonylphosphine complexes in terms of eq 9 , where the first term represents

$$\langle A^P \rangle = A^P{}_s \rho_P{}^{3s} + Q^P{}_{Cr} \rho_{Cr}{}^{3d} + Q^P{}_P \rho_P{}^{3p} \qquad (9)$$

the contribution of P 3s spin density, $A^P{}_s = 4438 \times 10^{-4}$ cm^{-1},[21] the second term represents polarization of P ns orbitals by spin density on Cr, and the third term represents polarization of P ns orbitals by spin density in a P 3p orbital. From an analysis of the ^{31}P couplings, we obtained an estimate of the metal polarization term for phosphine complexes, $Q^P{}_{Cr} \approx -38 \times 10^{-4}$ cm^{-1}. Assuming negligible P 3s spin density, this term can be used to estimate the metal spin densities in the present phosphine complexes, ∼0.8−0.9, consistent with estimates from extended Hückel MO calculations. Since the phosphites have isotropic couplings $\sim 11 \times 10^{-4}$ cm^{-1} larger in magnitude than the phosphines, and $\rho_P{}^{3p} \approx 0.011$, assuming the same value of $Q^P{}_{Cr}$ and comparable metal spin densities for the phosphite complexes leads to $Q^P{}_P \approx -1000 \times 10^{-4}$ cm^{-1}. This value is almost certainly much too large in magnitude. A more likely explanation for the larger phosphite couplings is that $Q^P{}_{Cr}$ increases in magnitude with decreasing Cr−P bond length. Figure 3 shows a plot of $\langle A^P \rangle$ for $[Cr(CO)_2L(\eta\text{-}C_6Me_6)]^+$ as a function of Cr−P bond lengths for

(21) Morton, J. R; Preston, K. F. *J. Magn. Reson.* **1978**, *30*, 577.

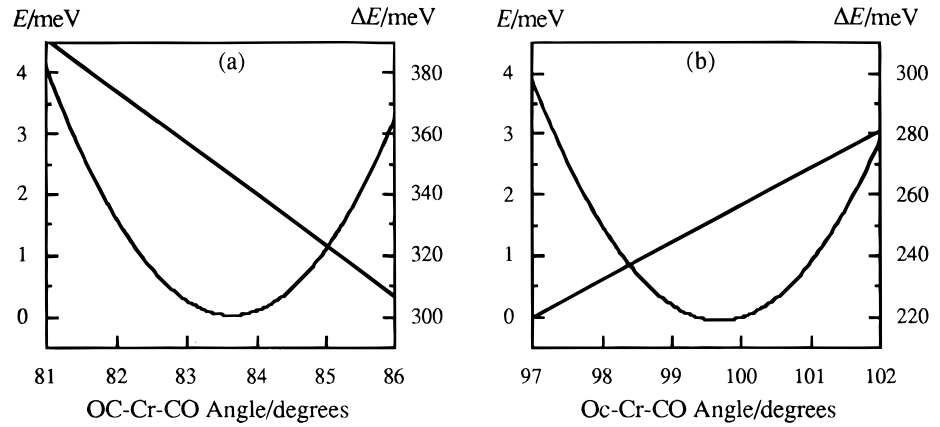

Figure 4. Plots of total energy and the SOMO/HOMO energy difference from EHMO calculations as functions of the OC−Cr−CO bond angle for $[Cr(CO)_2(PH_3)(\eta\text{-}C_5H_5)]$ in the $^2A''$ (a) and $^2A'$ (b) conformations found by Fortier, et al.[1]

Table 4. Width of g_z Distributions for Cr(I) Complexes

complex	g_Z	T/K	w_{high}[a]	w_{low}[a]	w_g	$w_g/\delta g_Z$
$[Cr(CO)_2(PEt_3\}(\eta\text{-}C_6Me_6)]^+$	2.109	90	8.8	3.9	0.0053	0.050
$[Cr(CO)_2(PPh_3)(\eta\text{-}C_6Me_6)]^+$	2.102	90	9.9	3.2	0.0062	0.062
$[Cr(CO)_2\{P(OEt)_3\}(\eta\text{-}C_6Me_6)]^+$	2.111	90	14.0	3.7	0.0090	0.082
$[Cr(CO)_2\{P(OPh)_3\}(\eta\text{-}C_6Me_6)]^+$	2.112	90	14.4	3.4	0.0093	0.084
$[Cr(CO)_2(PMe_3)(\eta\text{-}C_5Ph_5)]$[b]	2.104	120	11.0	2.2	0.0071	0.070
$[Cr(CO)_2(PPhMe_2)(\eta\text{-}C_5Ph_5)]$[b]	2.106	120	8.9	2.4	0.0057	0.055
$[Cr(CO)_2P(OMe)_3\}(\eta\text{-}C_5Ph_5)]$[b]	2.130	125	25	2.5	0.017	0.13

[a] Gaussian widths in units of gauss. [b] Data from ref 8.

$[Cr(CO)_5L]$.[22−24] While the correlation is monotonic, suggesting that the bond length dependence is real, the phosphine and phosphite points, taken separately, suggest a smaller bond length dependence than that observed when phosphines and phosphites are compared. Thus either Cr−P(OR)$_3$ bonds are intrinsically more easily spin polarized than Cr−PR$_3$ bonds or Q^P_P is relatively large and negative; quite possibly, both explanations are correct. A negative sign is at first surprising since the comparable parameter for carbon is positive,[25] but we note that the analogous Qs are well-known to be negative for transition metals.

Line Width Effects in EPR Spectra of Cr(I) Complexes. Given our understanding of the origins of **g**-matrix anisotropy, discussed above, and the conclusion that environmental effects can lead to either of two ground states for $[Cr(CO)_2L(\eta\text{-}C_6Me_6)]^+$ and $[Cr(CO)_2L(\eta\text{-}C_5Ph_5)]$, it is not difficult to understand the reason for the anomalous widths of the low-field spectral features corresponding to g_Z. Small deviations of the OC−Cr−CO bond angle from the average value lead to substantial changes in the SOMO/HOMO energy difference. EHMO calculations[6] were used to model the effect of small deviations from the optimum $^2A''$ and $^2A'$ conformations of Fortier et al;[1] the results are shown in Figure 4. The SOMO/HOMO energy difference changes about 5.0 and 4.7% per degree change in bond angle for the $^2A''$ and $^2A'$ conformations, respectively. (The difference in energies of the SOMO and the next filled MO also varies with angle, but by a much smaller relative amount.) Since the SOMO/HOMO energy difference appears in the denominator of the first terms of eqs 2 and 3 for $g_{xx} - g_e$, $g_{zz} - g_e$, and g_{xz}, these parameters are expected to vary with bond angle by about the same amount. After matrix diagonalization, the effect is concentrated in the maximum **g**-component, g_Z; $g_Z - g_e$ then is expected to vary by about 9−10% per degree.

There is literature precedent for the kind of orientation-dependent line width effect seen in the present work. Thus, for example, Imagawa[26] found orientation- and quantum number-dependent line widths in spectra of Cu^{2+} in various oxide glasses which he attributed to a distribution of ligand field strengths in the glasses. Similarly, Griscom[27] found that the $g_\perp$ features were anomalously broad in spectra of Cl and Br atoms in irradiated alkali halides and attributed the broadening to a distribution in the spacing of the p_z and $p_{x,y}$ energy levels, which is responsible for the departure of $g_\perp$ from g_e. In general, powder or frozen solution ESR spectra are subject to environmental variations which may affect one or more of the spin Hamiltonian parameters.[28]

Gaussian width parameters[29] are given in Table 4 for the low-field and high-field features in spectra of $[Cr(CO)_2L(\eta\text{-}C_6Me_6)]^+$ and $[Cr(CO)_2L(\eta\text{-}C_5Ph_5)]$. We assume that all spectral features are subject to the same inhomogeneous broadening mechanism (of unspecified origin) and that the excess broadening of the low-field features may be computed using eq 10, where we note

$$w_{excess} = \sqrt{w_{low}^2 - w_{high}^2} \qquad (10)$$

that Gaussian line width contributions combine as the

(22) Cr−P bond lengths for $[Cr(CO)_5(PPh_3)]$ and $[Cr(CO)_5\{P(OPh)_3\}]$ are from X-ray structures.[23] Bond lengths for the PEt$_3$ and P(OEt)$_3$ analogs were estimated from the experimental values for PPh$_3$ and P(OPh)$_3$ using the molecular mechanics results of Lee and Brown.[24]

(23) Plastus, H. J.; Stewart, J. M.; Grim, S. O. *Inorg. Chem.* **1973**, *12*, 265.
(24) Lee, K. J.; Brown, T. L. *Inorg. Chem.* **1992**, *31*, 289.
(25) Karplus, M.; Fraenkel, G. K. *J. Chem. Phys.* **1961**, *35*, 1312.
(26) Imagawa, H. *Phys. Status Solidi* **1968**, *30*, 469.
(27) Griscom, D. L. *Solid State Commun.* **1972**, *11*, 899.
(28) Taylor, P. C.; Baugher, J. F.; Kriz, H. M. *Chem. Rev.* **1975**, *75*, 203.

(29) The measured half-width at half-height is related to the Gaussian width parameter w by $\Delta B_{1/2} = (2 \ln 2)^{1/2} w$.

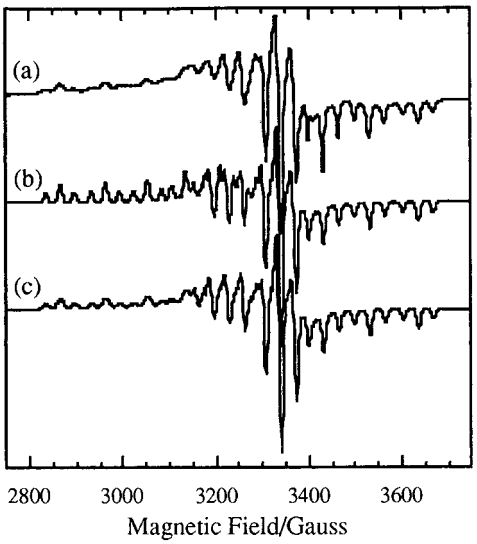

Figure 5. X-band EPR spectrum of $[Mn(CO)(dmpe)(\eta\text{-}C_5H_5)]^+$ in $CH_2Cl_2/C_2H_4Cl_2$ (1:1): (a) experimental spectrum at 120 K;[9] (b) simulation with parameters of Table 2 and constant 4.1 G Gaussian line widths; (c) simulation with constant 4.1 G line widths, $w_g = 0.0049$.

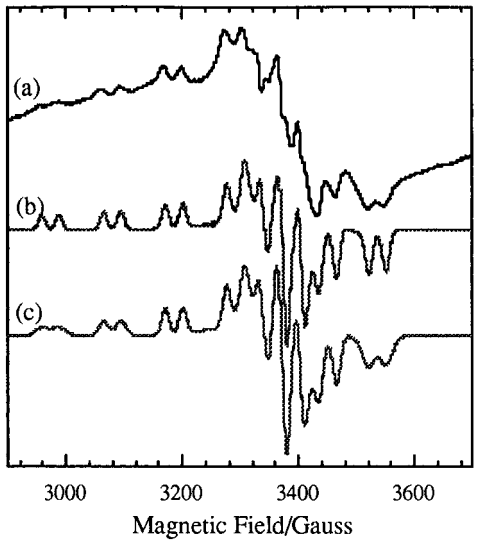

Figure 6. X-band EPR spectrum of $[Mn(CO)_2(PBu_3)(\eta^5\text{-}6\text{-}exo\text{-}PhC_6H_6)]^+$ in $CH_2Cl_2/C_2H_4Cl_2$ (1:1). (a) Experimental spectrum at 120 K;[9] (b) simulation with parameters of Table 2 and constant 5.9 G Gaussian line widths; (c) simulation with constant 5.9 G line widths, $w_A = 4.0 \times 10^{-4}$ cm^{-1}.

square root of the sum of squares. The excess width is attributed to a distribution of g_Z values. Consider the resonant field for a molecule oriented with the Z axis along the field, $B = h\nu/g_Z\mu_B$. The contribution to the observed width of the feature then is given by eq 11,

$$w_{\text{excess}} = w_g|\partial B/\partial g_z| = \frac{w_g B}{g_z} \tag{11}$$

where w_g is the width of the g_Z distribution, presumed to be Gaussian. Values of w_g, computed using eq 11, are given in Table 4. The quantity $w_g/(g_Z - g_e)$, a measure of the relative width of the g_Z distribution, is on the order of 0.05−0.07 for the phosphine complexes and 0.08−0.13 for the phosphites. Comparison with the EHMO results suggests a solvation-induced bond angle distribution with a width on the order of 1−2°. Note that the phosphine and phosphite complexes show somewhat different line width effects, consistent with the difference in ground state deduced from analysis of the ^{31}P hyperfine matrices.

If the above explanation is correct, the line width effect should be solvent- and temperature-dependent. For $[Cr(CO)_2L(\eta\text{-}C_5Ph_5)]$,[8] the low-field line widths increase with increasing temperature for L = PMe_3 and $P(OMe)_3$ but decrease for L = $PPhMe_2$; the line width effect for L = $P(OMe)_3$ is much greater in $CH_2Cl_2/C_2H_4Cl_2$ than in toluene.[8] These effects are consistent with the steric requirements of the very crowded C_5Ph_5 complexes. Thus, smaller solvent molecules are more likely to affect the OC−Cr−CO bond angle, and the $PPhMe_2$ ligand is more likely to exclude solvent molecules from the crucial region, particularly when its vibrational amplitude increases. A more extensive study might well lead to further insights into the nature of solvation in frozen solutions.

Line Width Effects in EPR Spectra of Mn(II) Complexes. Spectra of the Mn(II) complexes fall into two categories. Spectra of $[Mn(CO)(dmpe)(\eta^5\text{-}C_5H_5)]^+$ and other cyclopentadienyl complexes have anomalously broad low-field "parallel" features, but the width increases with decreasing $|m_I|$, the ^{55}Mn nuclear spin quantum number, as shown in Figure 5a. Spectra of $[Mn(CO)_2(PBu_3)(\eta^5\text{-}6\text{-}exo\text{-}PhC_6H_6)]^+$ and other 6-*exo*-PhC_6H_6 complexes also have broad parallel features, but the widths increase with increasing $|m_I|$ at both ends of the spectrum, as shown in Figure 6a. In either case, simulations based on constant line widths, shown in Figures 5b and 6b, give poor accounts of the spectra.

The interpretation of the line width effects in the spectrum of $[Mn(CO)(dmpe)(\eta^5\text{-}C_5H_5)]^+$ is complicated by the presence of ^{55}Mn hyperfine coupling and the fact that the principal axes of the g and ^{55}Mn hyperfine coupling matrices are displaced in the xz plane by 45°. Because of the noncoincidence of the **g**- and **A**-matrix principal axes, the various parallel features correspond to different orientations of the magnetic field in the **g**-matrix principal axis coordinate system; these orientations are given in Table 5a. Thus if the excess width is associated with orientation along the **g**-matrix Z axis, we expect the widths to increase in the order $m_I = -^1/_2 < -^3/_2 < -^5/_2 \ll +^5/_2 < +^3/_2 < +^1/_2$, and this is indeed observed. Including the ^{55}Mn hyperfine interaction, the field position of a spectral feature can be written as in eq 12, where k is the (angle-dependent) hyperfine

$$B = \frac{h\nu}{g_{\text{eff}}\mu_B} - \frac{km_I}{g_{\text{eff}}\mu_B} \tag{12}$$

coupling and g_{eff} is given by eq 13. Differentiating with

$$g_{\text{eff}} = \sqrt{(g_X{}^2\cos^2\phi + g_Y{}^2\sin^2\phi)\sin^2\theta + g_Z{}^2\cos^2\theta} \tag{13}$$

$$\frac{\partial B}{\partial g_Z} = -\frac{Bg_Z}{g_{\text{eff}}{}^2}\cos^2\theta \tag{14}$$

respect to g_Z, eq 14, we see that the line width sensitivity of a feature depends not only on the orientation in the field but also on the magnitude of the field. Values of $\partial B/\partial g_z$ are shown in Table 5a. Taking the width of

Table 5. Analysis of Widths of "Parallel" Features in Spectra of Mn(II) Complexes

(a) $[Mn(CO)(dmpe)(\eta\text{-}C_5H_5)]^+$ (115 K)

	m_I					
	$^5/_2$	$^3/_2$	$^1/_2$	$-^1/_2$	$-^3/_2$	$-^5/_2$
$B_{\|\|}$/G	2865	2962	3053	3432	3532	3636
$\theta_{\|\|}$/	14.5°	9.4°	3.3°	86.4°	81.1°	76.6°
$\|\partial B/\partial g_z\|$/G	1240	1324	1392	8	46	105
w/G[a]	7.2	7.5	8.2	3.1	4.1	5.4
w_{excess}/G[a,b]	5.9	6.2	7.2		0	
w_g	0.0048	0.0047	0.0051			

(b) $[Mn(CO)_2(PBu_3)(\eta^5\text{-}6\text{-}exo\text{-}PhC_6H_6)]^+$ (115 K)

	m_I					
	$^5/_2$	$^3/_2$	$^1/_2$	$-^1/_2$	$-^3/_2$	$-^5/_2$
$B_{\|\|}$/G	2973	3080	3186	3388	3450	3537
$\theta_{\|\|}$/	7.2°	5.1°	3.6°	78.8°	59.5°	43.4°
$\|\partial B/\partial A_{z'}\|/10^4$ G cm	2.54	1.52	0.49	0.19	0.97	2.15
w/G[a]	11.6	7.6	6.6		6.3	10.8
w_{excess}/G[a,c]	10.0	4.8	3.0		2.2	9.0
$w_A/10^{-4}$ cm^{-1}	3.9	3.2	(6.1)		(2.3)	4.2

[a] Gaussian width parameter. [b] Assuming $w_{x,y} = 4.1$ G. [c] Assuming $w_{x,y} = 5.9$ G.

the $-^3/_2$ feature as w_{high} (the width of the $m_I = -^1/_2$ feature is anomalously narrow as a result of the destructive interference of a divergence feature), eq 10 gives the corrected widths, w_{excess}, listed in Table 5a. Equation 11 then leads to the values of w_g listed in the table. A simulation incorporating a Gaussian distribution of g_Z with $w_g = 0.049$ is shown in Figure 4c. The value of w_g obtained for $[Mn(CO)(dmpe)(\eta\text{-}C_5H_5)]^+$ is somewhat smaller than those obtained for the Cr(I) dicarbonyl complexes. This is expected since, for monocarbonyl complexes, both the SOMO and HOMO are expected to be of a′ symmetry with the a″ MO significantly lower in energy; thus solvent-induced changes in ligand bond angles are expected to have a smaller relative effect on the a′/a″ energy difference and thus on g_Z. Line width effects are considerably more pronounced in the spectrum of $[Mn(CO)_2(PPh_3)(\eta\text{-}C_5H_5)]^+$, consistent with a larger value of w_g comparable to those obtained for the Cr(I) phosphine complexes.

The spectrum of $[Mn(CO)_2(PBu_3)(\eta^5\text{-}6\text{-}exo\text{-}PhC_6H_6)]^+$, shown in Figure 5, is typical of the 6-*exo*-PhC_6H_6 complexes in showing an increase in the width of the parallel features with increasing $|m_I|$. (The monocarbonyl complexes show a similar, but usually considerably smaller, effect.) Although there may be a contribution from the g_Z distribution, the major effect here appears to be a distribution in $A_{Z'}$. Because of the noncoincidence of the **g**- and **A**-matrix principal axes, an analytical expression for $\partial B/\partial A_z$ is unwieldy, but this quantity is readily computed numerically using our powder pattern analysis program.[30] These derivatives are listed in Table 5b for each of the parallel features, together with the resonant fields, orientations of the magnetic field in the **g**-matrix axis system, and the measured Gaussian line widths. Assuming an underlying Gaussian line width contribution of 5.9 G (the value that gives the most consistent fit), we find that $A_{Z'}$ is distributed with a Gaussian width $w_A = (4 \pm 1) \times 10^{-4}$ cm^{-1}. A computer simulation with $w_A = 4 \times 10^{-4}$ cm^{-1} is shown in Figure 5c.

Extended Hückel MO calculations suggest that the SOMO in $[Mn(CO)_2(PBu_3)(\eta^5\text{-}6\text{-}exo\text{-}PhC_6H_6)]^+$ is of a′ symmetry and is significantly delocalized over the π-orbitals of carbons 1, 5, and 6 of the 6-exo-PhC_6H_6 ligand. This is consistent with the EPR parameters, in particular the average ^{55}Mn coupling, which is noticeably smaller than for the cyclopentadienyl analogs. EHMO calculations further suggest a marked dependence of the delocalization on the dihedral angle describing the tilt of C-6 out of the plane of the other five carbon atoms, increasing the Mn 3d spin density by ~1% per degree increase in the dihedral angle. The observed component widths suggest a distribution in $A_{Z'}$ of ~4%, suggesting a distribution of dihedral angle on the order of 4°. Variable solvation in the frozen solution thus appears to tilt the 6-*exo*-Ph group (and thus C-6) over a range of angles.

Conclusion

(1) $[Cr(CO)_2\{P(OEt)_3\}(\eta\text{-}C_6Me_6)]^+$ and $[Cr(CO)_2\{P(OPh_3\}(\eta\text{-}C_6Me_6)]^+$ in frozen CH_2Cl_2/THF have ^{2}A″ ground state configurations; for these complexes, the ^{31}P hyperfine anisotropy is adequately explained in terms of dipolar coupling of the ^{31}P nucleus to spin density on Cr and to a small spin density (~0.011) in the P $3p_y$ orbital resulting from π-backbonding.

(2) $[Cr(CO)_2(PEt_3)(\eta\text{-}C_6Me_6)]^+$, $[Cr(CO)_2(PPh_3\}(\eta\text{-}C_6Me_6)]^+$, and $[Cr(CO)_2(PPhMe_2)(\eta\text{-}C_5Ph_5)]$ in frozen solution have ^{2}A′ ground state configurations; the ^{31}P hyperfine anisotropy is accounted for by dipolar coupling of the ^{31}P nucleus to spin density on Cr only.

(3) For both the phosphine and phosphite complexes, the major axis of the ^{31}P hyperfine interaction is along the Cr−P bond which differs from the **g**-matrix principal *z*-axis by 52−63°, i.e., the C_5−Cr−P or C_6−Cr−P angle complement plus β_g.

(4) The anomalous broadening of the low-field features of EPR spectra of $[Cr(CO)_2L(\eta\text{-}C_6Me_6)]^+$, $[Cr(CO)_2L(\eta\text{-}C_5Ph_5)]$, $[Mn(CO)_2L(\eta\text{-}C_5H_5)]^+$, and $[Mn(CO)L_2(\eta\text{-}C_5H_5)]^+$ can be accounted for by variable distortion of the OC−M−CO bond angle by solvation in frozen solutions while the qualitatively different line width effects observed in spectra of $[Mn(CO)_2L(\eta^5\text{-}6\text{-}exo\text{-}PhC_6H_6)]^+$ and $[Mn(CO)L_2(\eta^5\text{-}6\text{-}exo\text{-}PhC_6H_6)]^+$ suggest variable solvent displacement of C-6 relative to the mean plane of the coordinated C atoms, presumably through solvent interaction with the 6-*exo*-Ph group.

Acknowledgment. We thank the EPSRC for funds to purchase an EPR spectrometer at the University of Bristol, the National Science Foundation (Grant CHE-9123178), and the donors of the Petroleum Research Fund, administered by the American Chemical Society, for support of the research at Marshall University. We are indebted to a reviewer for suggesting the bond length dependence of the hyperfine parameter, Q^P_{Cr}.

(30) DeGray, J. A.; Rieger, P. H. *Bull. Magn. Reson.* **1987**, *8*, 95.

OM970251P